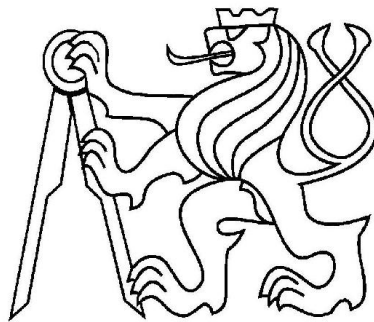


Czech Technical University in Prague  
Faculty of Nuclear Sciences and Physical  
Engineering



## Research work

Study of hadron correlations with high  
transverse momentum in  $d+Au$   
collisions at RHIC

Prague, 2010

Author: Michal Sloboda

Supervisor: RNDr. Jana Bielčíková, Ph.D.



## Prohlášení

Prohlašuji, že jsem svůj výzkumný úkol vypracoval samostatně a použil jsem pouze podklady (literaturu, projekty, SW atd.) uvedené v příloženém seznamu.

Nemám závažný důvod proti užití tohoto školního díla ve smyslu §60 Zákona č.121/2000 Sb., o právu autorském, o právech souvisejících s právem autorským a o změně některých zákonů (autorský zákon).

V Praze dne

## **Acknowledgements**

First of all, I am very grateful to my supervisor Jana Bielčíková, for her invaluable help, motivation, patience, and support during creation of this work. I am also very thankful to Jan Kapitán for his precious advices and to Jan Rusňák for languages corrections.

*Názov práce:* **Studium korelacií hadronů s vysokou příčnou hybností v d+Au srážkách na urychlovači RHIC**

*Autor:* Bc. Michal Sloboda

*Obor:* Jaderné inženýrství

*Zameranie:* Experimentální jaderná fyzika

*Druh práce:* Výzkumný úkol

*Vedúci práce:* RNDr. Jana Bielčíková, Ph.D., Ústav jaderné fyziky Akademie věd České republiky, v. v. i.

*Konzultant:* Mgr. Jan Kapitán

*Abstrakt:* Azimutálne korelácie sú dôležitým zdrojom informácií pre štúdium ultra-relativistických zrážok ťažkých iontov, pri ktorých sa produkuje veľké množstvo častíc. Zámerom práce je oboznámiť sa s metódou dvoj-časticových korelácií a ich praktickou aplikáciou na dáta z d+Au zrážok pri energii  $\sqrt{s_{NN}} = 200$  GeV nameraných v experimente STAR na urychlovači RHIC v roku 2008.

*Kľúčové slová:* dvoj-časticové korelácie, STAR, jadro-jadrové zrážky, hadróny

*Title:* **Study of hadron correlations with high transverse momentum in d+Au collisions at RHIC**

*Author:* Bc. Michal Sloboda

*Supervisor:* RNDr. Jana Bielčíková, Ph.D.

*Consultant:* Mgr. Jan Kapitán

*Abstract:* Azimuthal correlations are an important source of information for the study of ultra-relativistic heavy ion collisions, which produce a large amount of particles. The aim of this work is to become familiar with the method of two-particle correlations and their application to data from d+Au collisions at energy  $\sqrt{s_{NN}} = 200$  GeV measured in the STAR experiment at RHIC accelerator in 2008.

*Keywords:* two-particle correlations, STAR, nucleus-nucleus collisions, hadrons

# Contents

<b>1</b>	<b>Preface</b>	<b>8</b>
<b>2</b>	<b>Introduction</b>	<b>9</b>
2.1	Quark Gluon Plasma . . . . .	9
2.2	Heavy ion collisions . . . . .	10
2.3	Jets . . . . .	12
2.4	Azimuthal correlations . . . . .	12
<b>3</b>	<b>RHIC</b>	<b>16</b>
3.1	STAR detector . . . . .	18
3.1.1	Time Projection Chamber (TPC) . . . . .	19
3.1.2	Barrel Electromagnetic Calorimeter (BEMC) . . . . .	20
3.1.3	Time of Flight (TOF) . . . . .	20
3.1.4	Beam Beam Counter (BBC) . . . . .	20
3.1.5	Vertex Position Detector (VPD) . . . . .	21
3.1.6	Zero Degree Calorimeter (ZDC) . . . . .	21
3.1.7	Heavy Flavor Tracker (HFT) . . . . .	22
<b>4</b>	<b>Data Analysis</b>	<b>23</b>
4.1	Data sample . . . . .	23
4.2	Azimuthal correlation method . . . . .	23
4.3	Results . . . . .	23
<b>5</b>	<b>Summary and Conclusion</b>	<b>30</b>

# 1 Preface

Heavy-ion physics is one of the most dynamic branches of nuclear physics. Studies of hot and dense nuclear matter allow us to experimentally explore and identify the processes that took place in the first few moments of existence of the Universe. In the last decade, the experiments at the Relativistic Heavy Ion Collider (RHIC) at BNL have investigated properties of this hot and dense matter.

In central Au+Au collisions at  $\sqrt{s_{NN}} = 200$  GeV, the experiments at RHIC observe a large suppression of production of high transverse momentum ( $p_T$ ) particles, in comparison with the p+p and d+Au data. One of the tools to study this suppression are azimuthal correlations. In this research work di-hadron correlations in d+Au collisions at  $\sqrt{s_{NN}} = 200$  GeV are investigated using data measured by the STAR experiment. This measurement is an important baseline for nuclear-nuclear collisions.

After the introduction to the quark-gluon plasma and heavy ion collisions, the method of azimuthal correlations is described in Chapter 2. In Chapter 3 the RHIC facility and the STAR detector are described. In Chapter 4 the results of the analysis and conclusion are presented.

## 2 Introduction

### 2.1 Quark Gluon Plasma

The Quantum Chromodynamics (QCD) is a fundamental theory describing strong interactions among quarks and gluons. QCD has two special features:

**Confinement** refers to the fact that the force between quarks does not allow them to be free, no free colour-charged particle exists. Quarks have another quantum number - color. Quark's color may be one of three states: "red", "blue" and "green". In agreement with the QCD quarks are colorless objects - baryons (3 quarks: RGB) and mesons (quark-antiquark:  $R\bar{R}$ ,  $G\bar{G}$ ,  $B\bar{B}$ ). The force, that binds quarks increases with distance, if the distance between quarks reaches  $\sim 1$  fm, then the stored potential energy is sufficient to create a new quark-antiquark pair (meson). It follows that it is not possible to release the colorful quark, because it would require infinite amount of energy.

**Asymptotic freedom** means that in very high-energy reactions, quarks and gluons interact very weakly. This means that in close proximity they behave almost as free particles. This behavior can be observed in high energy collisions, where large momentum is transferred.

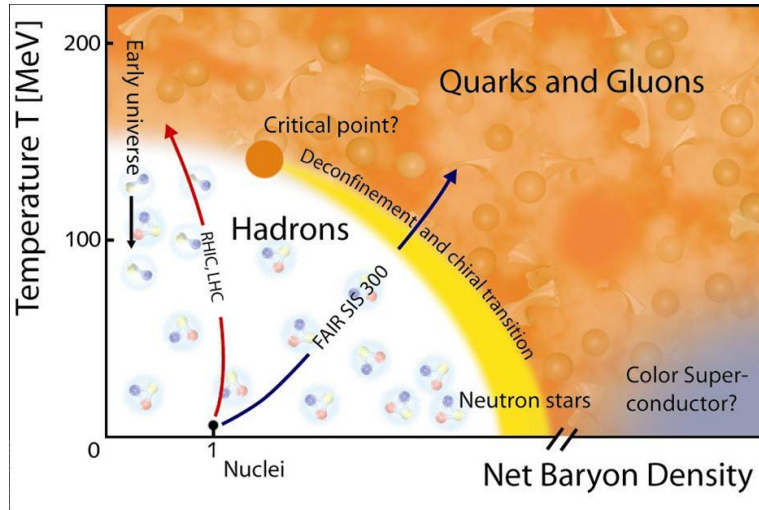


Figure 1: The QCD phase diagram.

Quark-gluon plasma (QGP) is a new phase of matter, in which where quarks and gluons are not restricted by the phenomenon of color confinement and they are free. The phase diagram is shown in Figure 1. Calculations of the lattice QCD expect the phase transition from nuclear matter to quark-gluon plasma at the critical temperature  $T \sim 170$  MeV what corresponds to energy density of  $1 \text{ GeV}/fm^3$ . The revelation of the new state of matter was announced by a press release on the 10th of February, 2000 [11].

Under certain conditions of high temperature  $T$  and/or high density  $\rho$  the QGP can be found in three places:

- (i) in the early Universe
- (ii) at the center of compact stars
- (iii) in the initial stage of colliding heavy nuclei at high energies

(i) QGP existed in the early Universe until about  $10^{-5}$  s after the Big Bang. At the time  $10^{-5} - 10^{-4}$  s after the Big Bang the QGP in space underwent the phase transitions.

(ii) At the cores of superdense stars such as quark stars and neutron stars. In the center of neutron stars density is sufficient to generate a cold quark matter, this matter mostly consists of  $u$ ,  $d$ , and  $s$  quarks.

(iii) In the initial stage of the "Little Bang" at relativistic nucleus-nucleus collisions. When the center of mass energy per nucleon exceeds 100 GeV (no strong boundary), the colliding nuclei pass through each other and produce matter with high energy density and high temperature[2].

## 2.2 Heavy ion collisions

Heavy ion collisions are a very useful experimental instrument to examine the properties of matter under extreme conditions of high density and temperature. Collisions can be classified according to the geometry in transverse plane. Head-on collisions with a large overlap are called central collisions, whereas those with few participant nucleons<sup>1</sup> are called peripheral (non-

---

<sup>1</sup>nucleons in the overlapping region

central) collisions [Figure 2]. The centrality of the collision is determined by the impact parameter<sup>2</sup>.

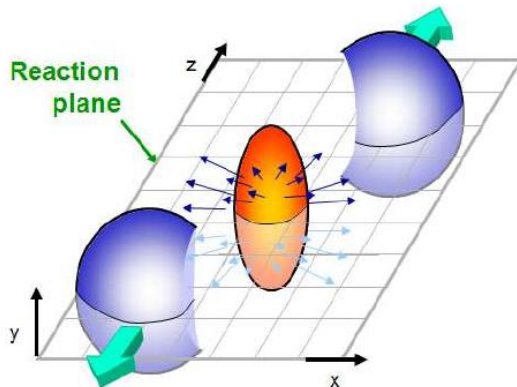


Figure 2: Scheme of non-central nuclear collision.

The main goal of ultrarelativistic collisions is to explore the phase transition from hadron gas to QGP at high temperatures. Low-energy collisions study relativistic nuclear matter at lower temperatures but higher baryon densities. The right part of Figure 3 shows the space-time evolution of QCD matter under conditions sufficient for QGP creation in heavy ion collision.

In the earliest moments after the collision, quarks and gluons are released from nucleons as a reason of high temperature and energy in the collision area and heavy quarks and the most energetic partons are produced. They will later fragment into jets. After  $10^{-24}$  s, quarks and gluons thermalize and the energy density is sufficient to produce QGP. The high pressure cause expansion of the QGP and its cooling. At some point the temperature drops below the critical temperature, deconfinement is no longer possible and the partons form into hadrons again. Most of the observed particles are created at this moment. Next stage is a hadron gas (results from the hadronization of the QGP), which still allows interactions between the hadrons. Final stage is freeze-out, where species of hadrons do not change anymore. Hadrons emerging from the freeze-out are observed in detectors. The knowledge of the distribution of hadrons provides us indirect information about QGP formation and about various stages of nuclei collision.

---

<sup>2</sup>is the perpendicular distance to the closest approach if the projectile were undeflected

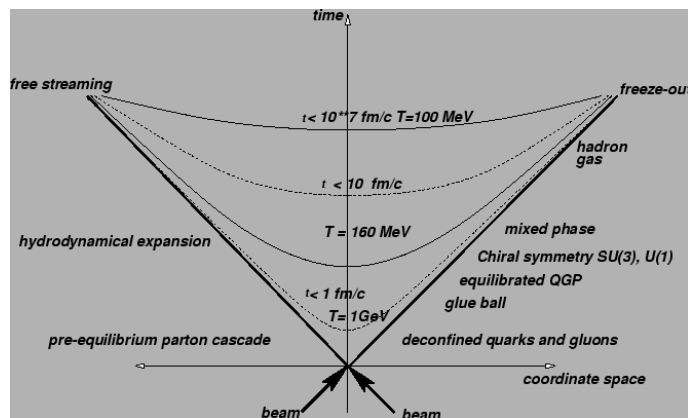


Figure 3: One-dimensional space-time picture of a nucleus-nucleus collision.

### 2.3 Jets

Jets are narrow sprays of hadrons and other particles, produced during collision of atomic nuclei from quarks and gluons as a result of fragmentation and hadronization process. Quarks and gluons cannot exist freely, therefore the scattered partons will transform into a cluster of hadrons that are accessible to measurements. These clusters of spatially correlated particles (jets) carry information about the original parton due to the momentum and energy conservation. Jets are also considered a good probe of the QCD matter created in the collision. In nucleus-nucleus collisions they are however difficult to be separated from underlying event. In jet analysis, it is essential to understand particular steps taken during their creation, from hard-scattering process, in which are created partons with high  $p_T$ , through fragmentation and hadronisation. The transverse shape of jet is defined as the projection of particle's momentum to the plane perpendicular to the jet axis:  $j_T = p_{hadron} \cdot \sin\theta$ . The jet containing lower  $p_T$  particles is wider and has higher  $j_T$  values. Low  $j_T$  values represent particles which form a narrow cone.

### 2.4 Azimuthal correlations

Generally jets are produced in pairs that are back-to-back in the transverse plane and are separated by an azimuthal distance  $\Delta\varphi \approx \pi$ . In case of the proton-proton collision, the hadron jet can be directly observed and recon-

structured [Figure 4]. The large multiplicity of particles in central heavy ion collision makes full jet reconstruction in practice very difficult [Figure 5]. Therefore azimuthal correlations between a trigger particle with very high transverse momentum, and associated high  $p_T$  particles from the same event are commonly used. The two-particle azimuthal correlations allow only the statistical jet observation.

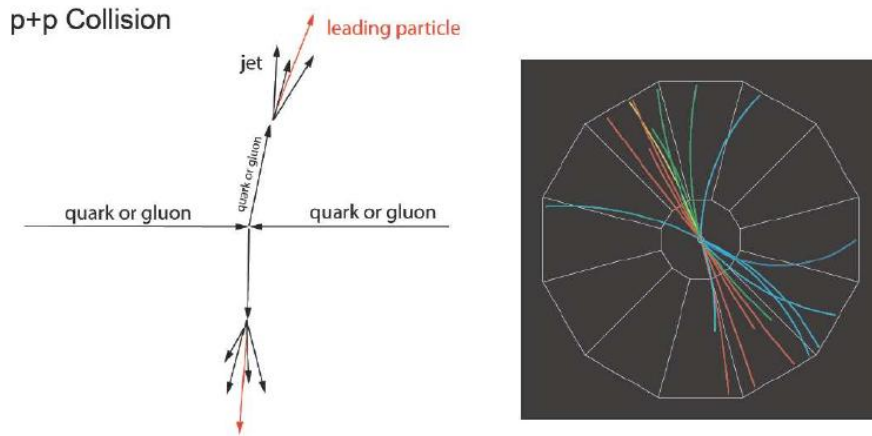


Figure 4: On the left cartoon of the central p+p collision and on the right the p+p collision recorded by the STAR TPC.

At first the leading (trigger) particle (i.e. particle with the highest transverse momentum  $p_T$  in event) is selected. Subsequently the angle  $\Delta\phi$  between the leading particle and other particles (associated) incurred during the collision is determined and it holds:  $p_T^{ASOC} < p_T^{TRIG}$ .

In the Figure 6 one can see azimuthal correlation function. This function has two peaks, one is in  $\Delta\phi = 0$ , and comes from the near-side jet (containing trigger particle). The second peak (away-side peak) is around  $\Delta\phi = \pi$  and comes from the opposite jet than the trigger particle. The background is formed by a correlation of the leading particle with particles belonging to no jet. One of the reasons why the near-side peak is higher and narrower, than peak from the away-side jet is that the near-side jet contains particle with the highest  $p_T$  - the trigger particle.

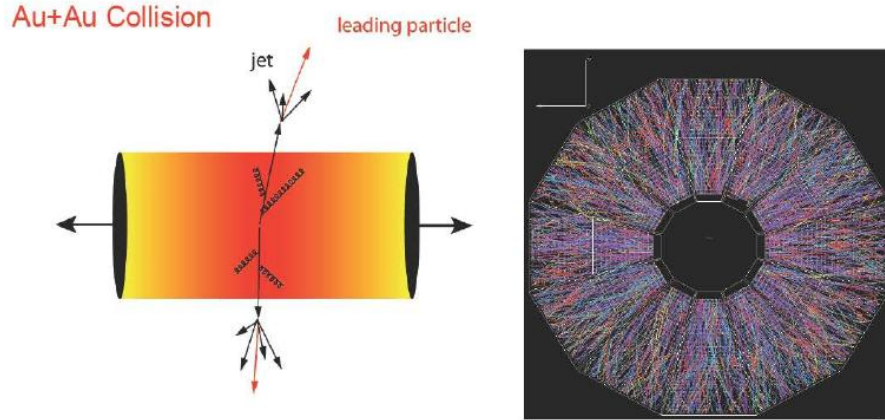


Figure 5: On the left cartoon of the central Au+Au collision and on the right the Au+Au collision recorded by the STAR TPC.

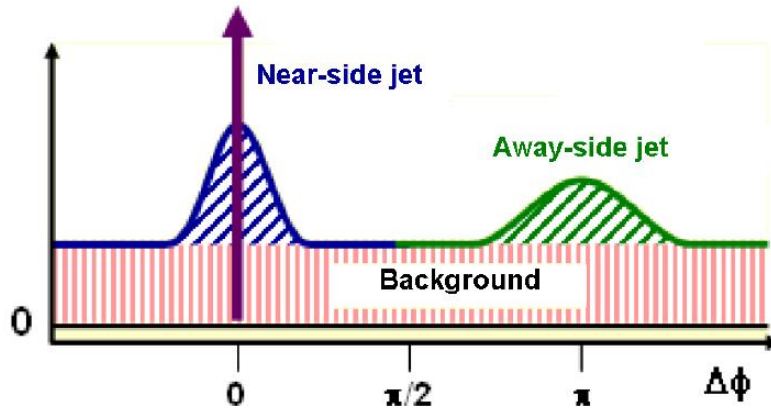


Figure 6: Azimuthal correlation function.

Azimuthal distributions for minimum bias and central d+Au collisions and for p+p collision shown in Figure 7(a) have both symmetric peaks. However, in Figure 7(b) near-side (left) peak is similar for all collisions, while the back-to-back (right) in central Au+Au shows a remarkable suppression relative to p+p and d+Au. This fact points to a jet energy loss in nuclear matter produced in Au+Au collisions.

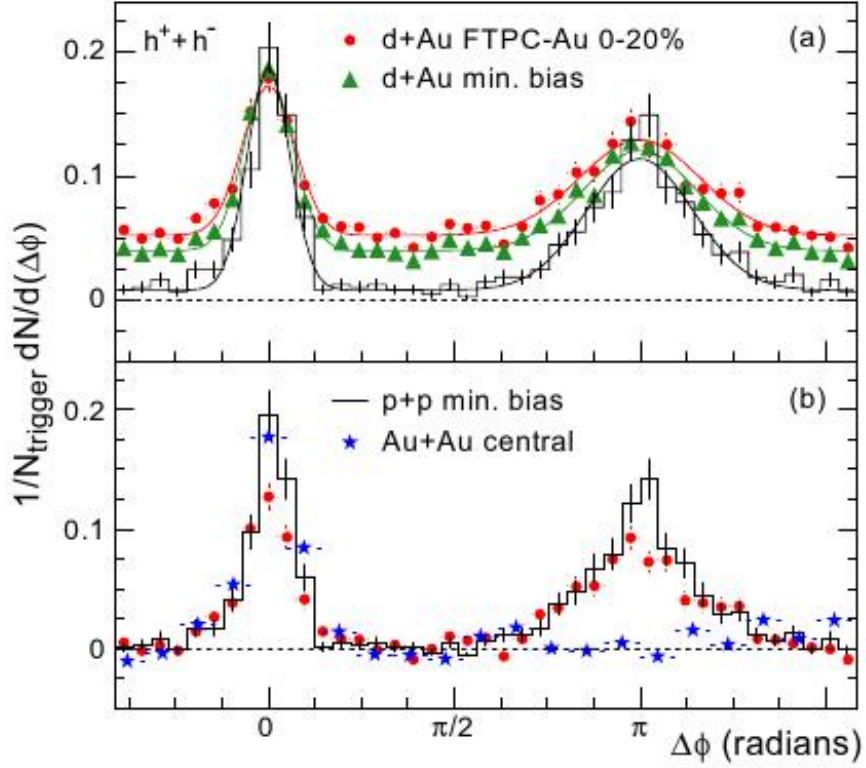


Figure 7: (a) Two-particle azimuthal distributions for minimum bias and central d+Au collisions and for p+p collision. (b) Comparison of two-particle azimuthal distributions for central d+Au collisions to those seen in p+p and central Au+Au collisions with  $p_T(\text{trig}) < 4, 6 > \text{GeV}$ ,  $p_T(\text{assoc}) < 2, 4 > \text{GeV}$ . [12]

### 3 RHIC

Relativistic Heavy Ion Collider (RHIC) has been in design since 1983, the own construction started in 1991 and it was finished in 1999. It started working in the summer of the year 2000. Until initiation of the LHC it was the biggest heavy-ion collider in the world. It is situated in Brookhaven National Laboratory on the Long Island, Upton NY. It is able to study polarized bunches of protons with energy up to  $\sqrt{s_{NN}} = 500\text{GeV}$  and bunches of  $d + Au$ ,  $Au + Au$ ,  $Cu + Cu$  up to energy  $\sqrt{s_{NN}} = 200\text{GeV}$ . Primary RHIC was designed to study nuclear matter at extremely high temperatures such as  $10^{12}\text{ K}$ , where theory predict a transition between hadronic matter and deconfined quark-gluon plasma(QGP). We can say that RHIC is not one accelerator, but two in one. Because it is composed of two separated rings which are 3834 m long. This unique construction allows us to collide two different particle species together.

Accelerating starts in the Van de Graaf accelerator for heavy ions and in Linac for protons. Electrons from negatively charged ions accelerated by the Van de Graaf are partially stripped off (by passing through a stripping foil) and the ions are accelerated by Tandem to 1 AMeV. Consequently the ions are transferred to Booster Synchrotron(high frequency circular accelerator), where they are accelerated to 95 AMeV. A foil at the Booster exit strips all atomic electrons except two bound K-shell electrons. The Alternating Gradient Synchrotron (AGS) accelerates the gold ions to energy 10.8 AGeV. Ions are completely stripped at the exit of the AGS. Afterwards ions are transported in AGS-To-RHIC (ATR) transfer line (to the RHIC). At the end of this line is a switching magnet, which sends the ion bunches to one of the two beam lines. In this two beam tubes particles are revolving in opposite directions. In case of protons acceleration process starts in Linac and continuous directly to Booster. Furthermore protons are accelerated in a similar way like the ions. RHIC has six intersection points, in four of them the detector systems are situated:

- BRAHMS
- PHOBOS
- PHENIX
- STAR

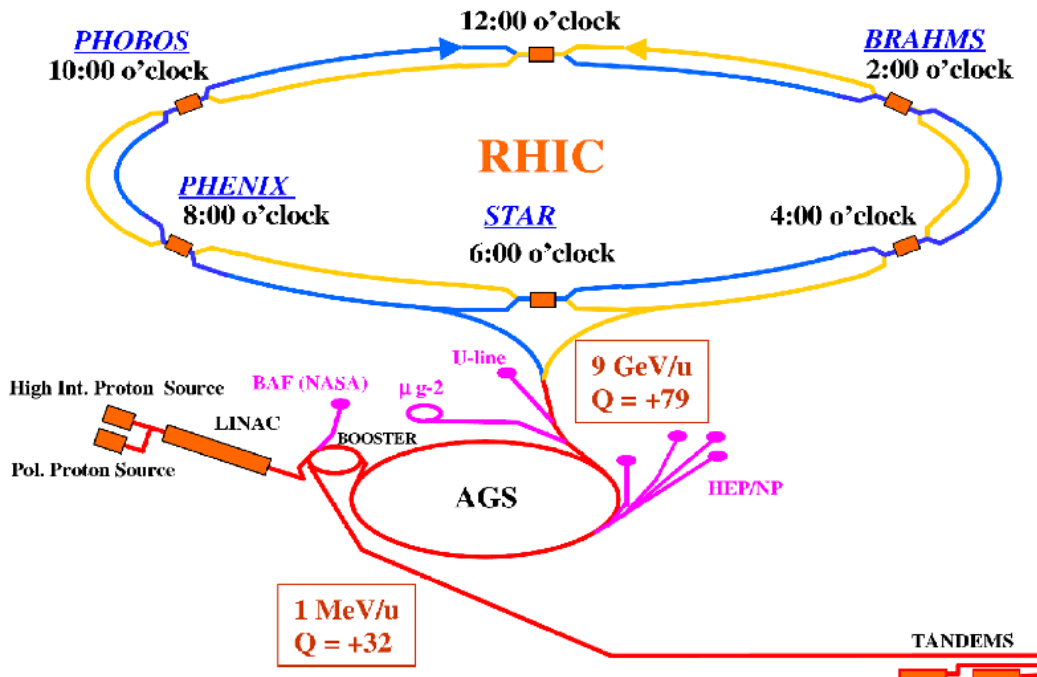


Figure 8: Scheme of the RHIC.

BRAHMS (Broad Range Hadron Magnetic Spectrometers) is one of smaller detectors. It is composed of a two-arm magnetic spectrometer: Mid rapidity spectrometer and Forward spectrometer. On the movable arms are located narrow gap dipole magnets, drift chamber planes, Čerenkov counters, time-of-flight and tracking detectors. The BRAHMS experiment was designed to measure charged hadrons and the properties of the highly excited nuclear matter.

PHOBOS consists of a two-arm magnetic spectrometer and several of ring multiplicity detectors. It measured quantities such as the temperature, size, and density of the fireball produced in the collision, which are important for the study a phase transition that might occur between quark-gluon plasma and ordinary matter. PHOBOS and BRAHMS were finished their operation in 2005 and 2006 respectively.

PHENIX (Pioneering High Energy Nuclear Interaction eXperiment) consist of central arm detectors, two muon arms and event characterization detectors. Its research goals are to study matter under extreme conditions of temperature and pressure, the examination of the quark–gluon plasma and the spin structure of proton.

### 3.1 STAR detector

STAR (Solenoidal Tracker At RHIC) belongs with PHENIX to large detectors at RHIC. The primary goals of STAR [5] are the following: search for signatures of quark-gluon plasma in central heavy ion collisions, search for value of critical point and to study the proton spin physics.

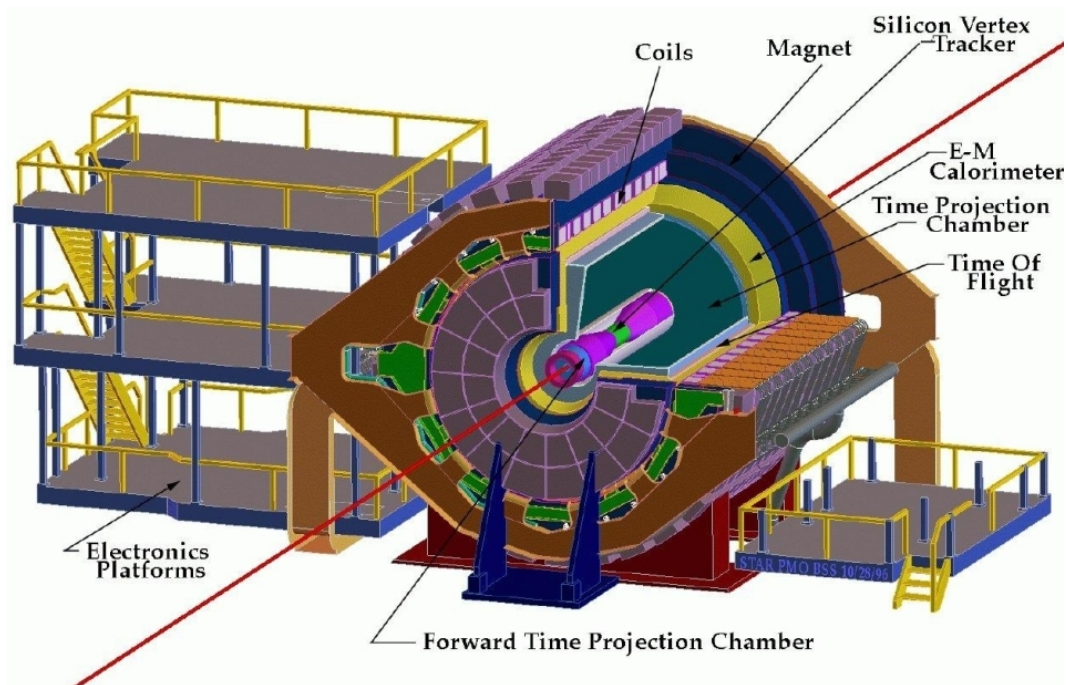


Figure 9: Cut of STAR detector with inner detector systems. [4]

The whole detector is inside a large solenoidal magnet which creates an uniform magnetic field of value 0.5 T, what allows the analysis of charged particles. The full azimuthal acceptance of STAR makes it very well suited for event-by-event characterizations of heavy ion collisions and for the detection of hadron jets. In following sections we will describe the most important detector subsystems of STAR detector.

### 3.1.1 Time Projection Chamber (TPC)

One of the most important parts of the STAR detector is the Time Projection Chamber (TPC), its primary tracking device. The TPC is situated at a radial distance from 50 to 200 cm from the beam axis, it's 4 m long cylinder filled with gaseous: methane (10%), argon (90%) at the atmospheric pressure and with a uniform electric field of 135 V/cm. It covers  $2\pi$  in azimuthal angle and from -1,8 to 1,8 in pseudo-rapidity. It can record the tracks of charged particles(ionize the gas around their tracks), measure their momenta, and identify the particles by measuring their energy loss ( $dE/dx$ ).

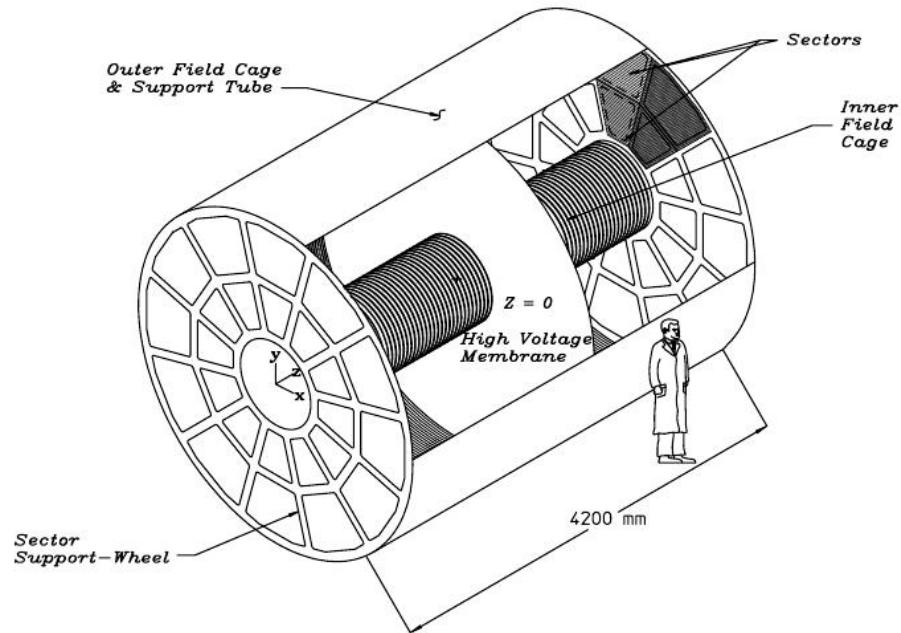


Figure 10: Illustration of the STAR TPC. [7]

The TPC is able to identify particles over a momentum range from 100 MeV to greater than 1 GeV. To drift the electrons it is necessary to have a uniform electric field generated by a thin conductive central membrane at the centre of the TPC, two concentric field cage cylinders and end-caps at zero potential. The end caps are grounded and they are divided into the 12 read-out sectors. Particles are registered by a Multi-Wire Proportional Chambers (MWPC), which provides amplification between 1000 and 3000. To neutral particles the TPC is insensitive. The track of an infinite-momentum particle passing through the TPC at mid-rapidity would be sampled by 45 pad rows, but a finite momentum track may not cross all 45 rows. From the end-cap MWPCs are obtained  $x$  and  $y$  coordinate of the tracks and  $z$  coordinate from the electron drift time. The  $dE/dx$  is extracted from the energy loss measured on up to 45 pad rows.

### 3.1.2 Barrel Electromagnetic Calorimeter (BEMC)

The STAR Barrel Electromagnetic Calorimeter (BEMC) consist of plastic scintillator and 41 layers of lead. The BEMC covers  $|\eta| < 1$  and  $2\pi$  in azimuthal angle. It includes 120 calorimeter modules, which are segmented into 40 towers. The full Barrel Calorimeter is segmented into a total of 4800 towers and all the towers are oriented in the direction of the interaction point. The BEMC is required for the reconstruction of the  $\pi^0$ , direct photons and  $W$  and  $Z$  decays.

### 3.1.3 Time of Flight (TOF)

The STAR TOF detector has been built to provide the particle identification. It measures the time it takes to a particle to fly through the TOF. It covers  $\pm 1$  in pseudorapidity, full azimuthal angle and has detection efficiency about 95%. From the time of flight together with the particle's momentum, it is possible to identify the particle. It contributed to measurements concerning charmed hadrons, non-photonic electron analysis and many others.

### 3.1.4 Beam Beam Counter (BBC)

There are two scintillator detectors around the beam pipe on both sides of the STAR detector, Beam Beam Counter West and East. It is a universal tool for polarized proton beam diagnostics. The BBC consists of two rings of scintillating tubes. In the STAR experiment it provides a crucial minimum

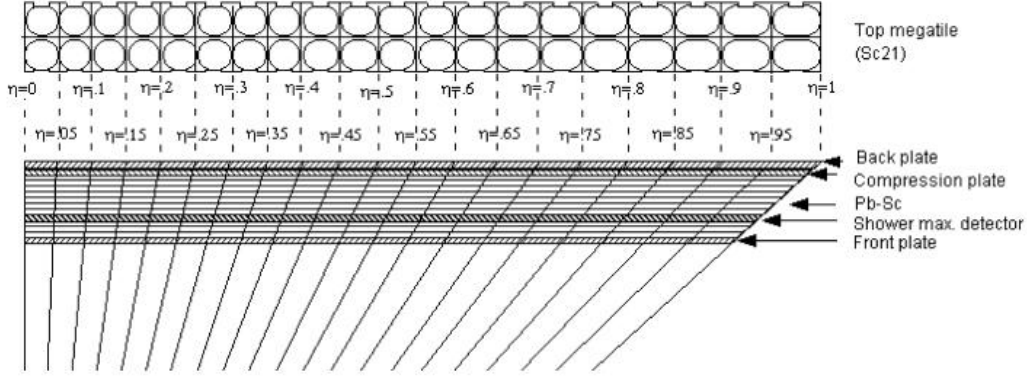


Figure 11: Side view of a BEMC module showing the projective nature of the towers. [8]

bias trigger for  $p + p$  collision. In terms of the trigger, the main difference between  $p + p$  and  $Au + Au, Cu + Cu$  collisions is the multiplicity.

### 3.1.5 Vertex Position Detector (VPD)

The VPD consists of two similar detector placed very close to the beam pipe outside the STAR magnet, approximately 5 m from the center of STAR. Each VPD consist of three fast plastic scintillator detectors with read-out by photomultiplier tubes. The VPD is very important for determination of the start time for TOF detector.

### 3.1.6 Zero Degree Calorimeter (ZDC)

ZDCs are hadron calorimeters. Each calorimeter is 10 cm wide to minimize the energy loss. Each of the RHIC experiments has a pair of Zero Degree Calorimeters (ZDC East and ZDC West). These are placed 18 m along the beam pipe on both side of the intersection region behind the dipole magnet. This dipole magnet deflects tracks of particles. Each ZDC consists of three modules. The individual module consists of a series of tungsten plates alternating with layers of wavelength shifting fibers. The ZDC coincidence is a minimal bias selection of heavy ion collisions and are used for beam monitoring, triggering, and locating interaction vertices.

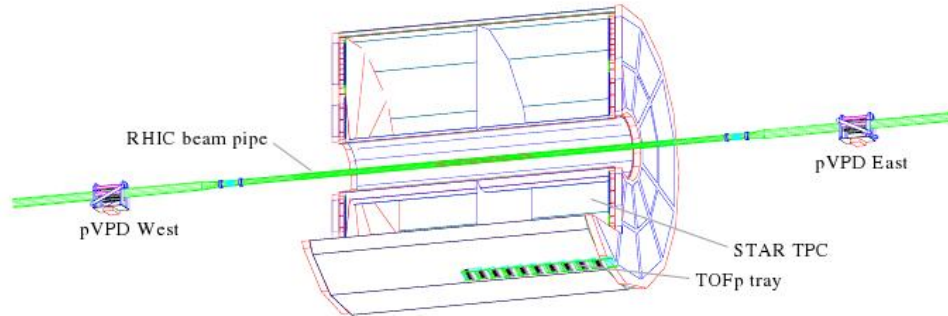


Figure 12: The locations of the VPD and TOF detectors in relation to the TPC and the beam pipe. [9]

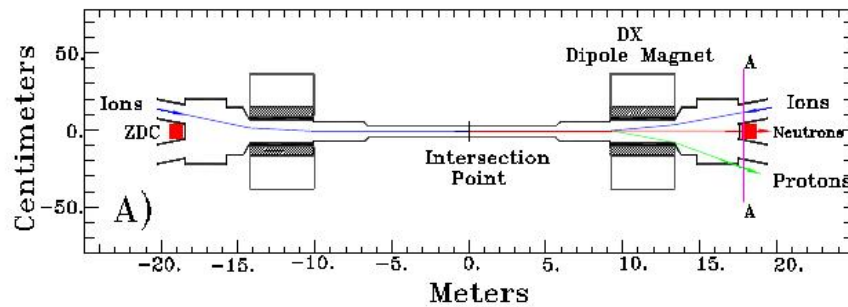


Figure 13: Location of both ZDC around the beam pipe. [15]

### 3.1.7 Heavy Flavor Tracker (HFT)

The Heavy Flavor Tracker is situated in the TPC to improve its tracking abilities. It consists of three detector systems, while one is already installed (Silicon Strip Detector) the other two are planned (Intermediate STAR Tracker, Pixel detector). It covers  $2\pi$  in azimuthal angle and from  $-1,0$  to  $1,0$  in pseudo-rapidity. The main purpose of the HFT is to measure the elliptic flow of charmed hadrons in the low  $p_T$  region and identify B-meson contributions in the region  $p_T > 4$  GeV/c.

## 4 Data Analysis

### 4.1 Data sample

For the analysis data from d+Au collisions at energy  $\sqrt{s_{NN}} = 200$  GeV from the RHIC Run 2008 are used. The total amount of collected events by STAR during the Run 08 was 46M events with minimum bias trigger<sup>3</sup> [14]. The trigger for minimum bias d+Au, was the VPD-ZDCE with a VPD vertex cut at +/- 30 cm.

### 4.2 Azimuthal correlation method

The necessary theoretical framework has been presented in previous sections. The charged tracks used in azimuthal correlations studies were reconstructed by the TPC and restricted in pseudorapidity  $|\eta| < 0.7$ . Figures 14-27 show the two-particle azimuthal distributions  $D(\Delta\phi)$ , defined as

$$D(\Delta\phi) \equiv \frac{1}{N_{trigger}} \frac{1}{\epsilon} \frac{dN}{d(\Delta\phi)}, \quad (1)$$

for minimum bias d+Au collisions, where  $N_{trigger}$  is the observed number of tracks satisfying the trigger requirement. The efficiency  $\epsilon$  for finding the associated particle is evaluated by embedding simulated tracks in real data. The azimuthal separations between the associated and the trigger particle are calculated ( $\Delta\phi = \phi^{trig} - \phi^{assoc}$ ) and used to construct the  $\Delta\phi$  distribution. Each associated particle contributes a value of  $1/\epsilon$  to the distribution.

### 4.3 Results

Figures 14-27 show the results of correlations functions. In comparison with Figure 7 we see both near- and away-side peaks. The suppression of high  $p_T$  particles in the d+Au collision (away-side peak) is not observed in comparison with the central Au+Au collisions at intermediate  $p_T \sim \langle 3, 6 \rangle$  GeV, where we see only near-side peak. Difference between d+Au and central Au+Au collisions reveals, that the suppression of high  $p_T$  particle is observed in matter produced in Au+Au and not in d+Au collisions. It follows that

---

<sup>3</sup>without using  $p_T$  trigger

in dense nuclear matter produced in central Au+Au collisions the jet suppression occurs. The  $p_T$  ranges used in this work are  $p_T(\text{trig}) < 3, 4 > \text{ GeV}/c$ ,  $p_T(\text{trig}) < 4, 6 > \text{ GeV}/c$  and  $p_T(\text{trig}) < 6, 10 > \text{ GeV}/c$  in order to select particles predominantly formed in a fragmentation process. The shape of correlation function can be describe by three gauss functions:  $f_1(x) = p_0 e^{-\frac{(x+\pi)^2}{2p_1^2}}$ ,  $f_2(x) = p_2 e^{-\frac{(x-0)^2}{2p_2^2}}$ ,  $f_3(x) = p_0 e^{-\frac{(x-\pi)^2}{2p_1^2}}$ . One ( $f_2(x)$ ) describe near-side peak and two ( $f_1(x)$  and  $f_3(x)$ ) are used for away-side peak. The following figures show azimuthal correlations of hadrons with high transverse momentum in the d+Au collisions at RHIC and scaled by  $1/0.89$ , where the efficiency for finding the associated particle is 89%. All azimuthal distributions are normalized per trigger particle for d+Au collisions.

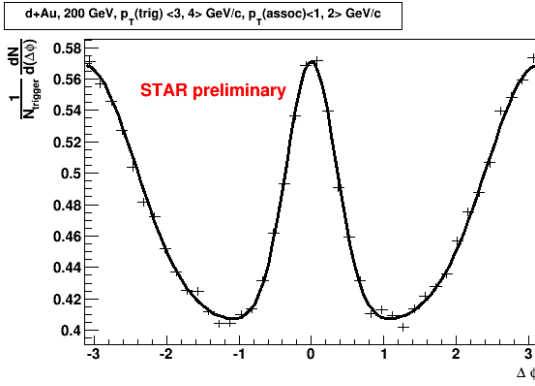


Figure 14: Azimuthal correlation with  $p_T(\text{trig}) < 3, 4 > \text{ GeV}/c$ ,  $p_T(\text{assoc}) < 1, 2 > \text{ GeV}/c$ .

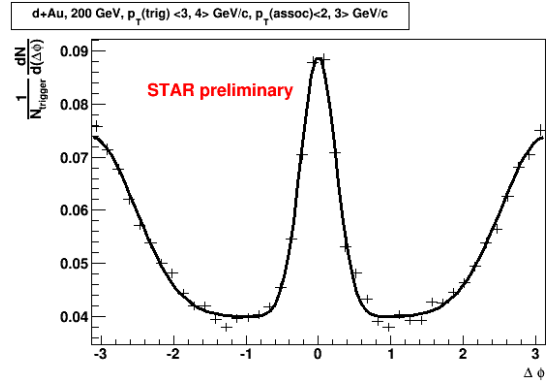


Figure 15: Azimuthal correlation with  $p_T(\text{trig}) < 3, 4 > \text{ GeV}/c$ ,  $p_T(\text{assoc}) < 2, 3 > \text{ GeV}/c$ .

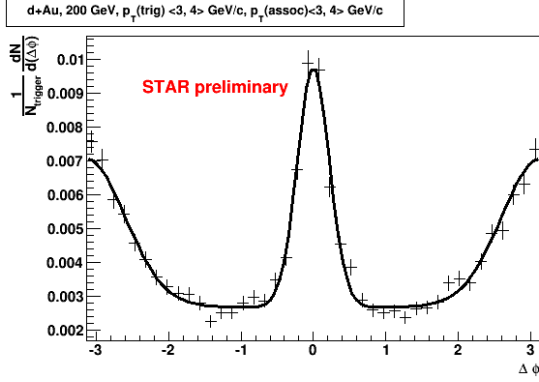


Figure 16: Azimuthal correlation with  $p_T(\text{trig}) < 3, 4 > \text{ GeV}/c$ ,  $p_T(\text{assoc}) < 3, 4 > \text{ GeV}/c$ .

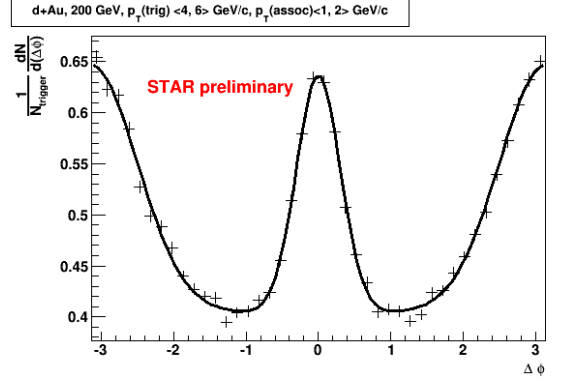


Figure 17: Azimuthal correlation with  $p_T(\text{trig}) < 4, 6 > \text{ GeV}/c$ ,  $p_T(\text{assoc}) < 1, 2 > \text{ GeV}/c$ .

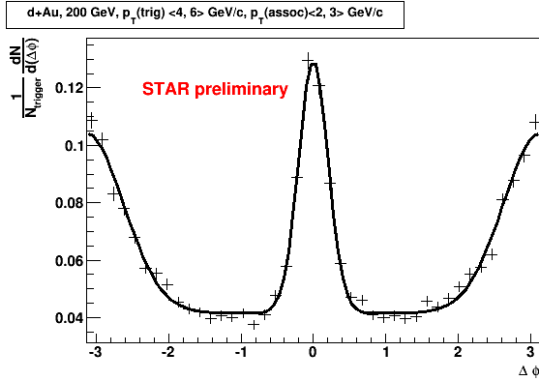


Figure 18: Azimuthal correlation with  $p_T(\text{trig}) < 4, 6 > \text{ GeV}/c$ ,  $p_T(\text{assoc}) < 2, 3 > \text{ GeV}/c$ .

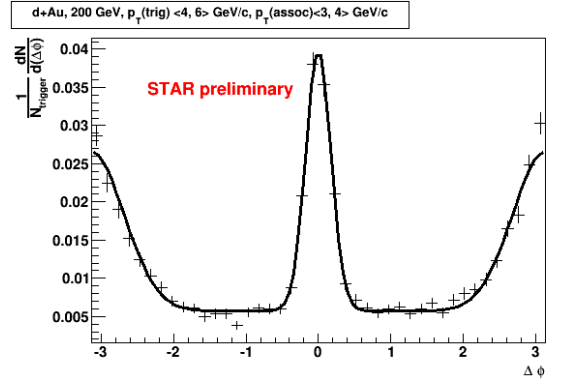


Figure 19: Azimuthal correlation with  $p_T(\text{trig}) < 4, 6 > \text{ GeV}/c$ ,  $p_T(\text{assoc}) < 3, 4 > \text{ GeV}/c$ .

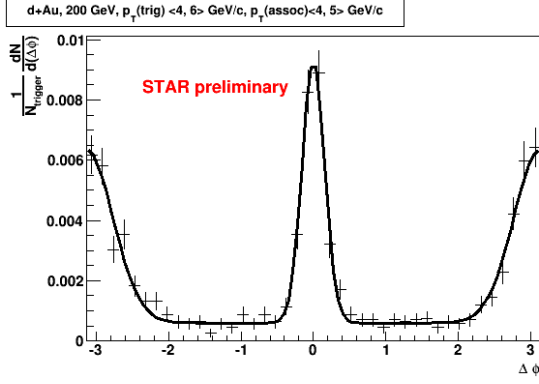


Figure 20: Azimuthal correlation with  $p_T(\text{trig}) <4,6>$  GeV/c,  $p_T(\text{assoc}) <4,5>$  GeV/c.

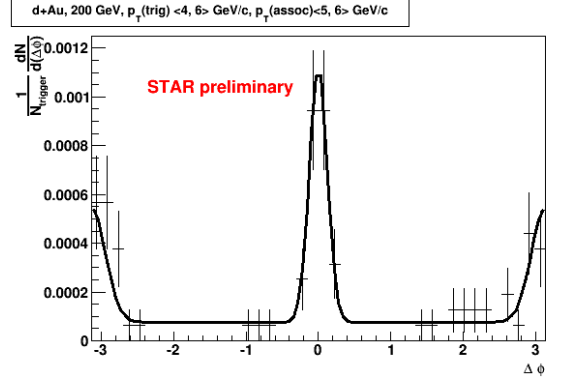


Figure 21: Azimuthal correlation with  $p_T(\text{trig}) <4,6>$  GeV/c,  $p_T(\text{assoc}) <5,6>$  GeV/c.

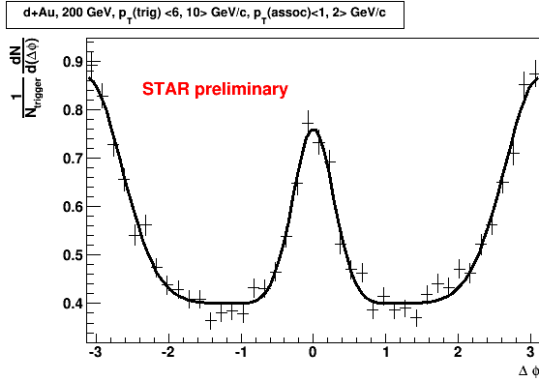


Figure 22: Azimuthal correlation with  $p_T(\text{trig}) <6,10>$  GeV/c,  $p_T(\text{assoc}) <1,2>$  GeV/c.

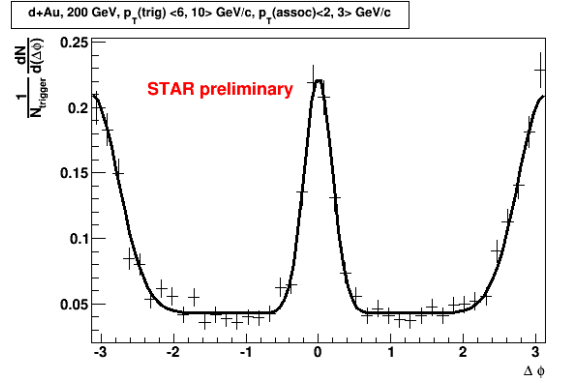


Figure 23: Azimuthal correlation with  $p_T(\text{trig}) <6,10>$  GeV/c,  $p_T(\text{assoc}) <2,3>$  GeV/c.

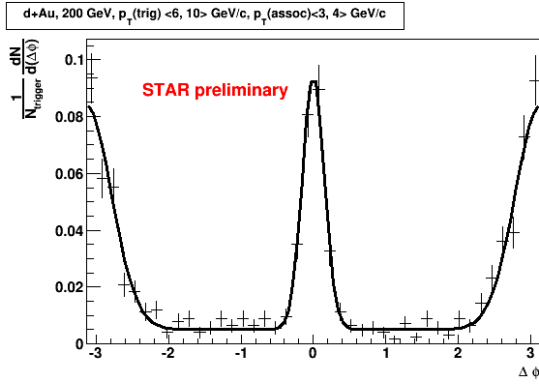


Figure 24: Azimuthal correlation with  $p_T(\text{trig}) <6,10>$  GeV,  $p_T(\text{assoc}) <3,4>$  GeV.

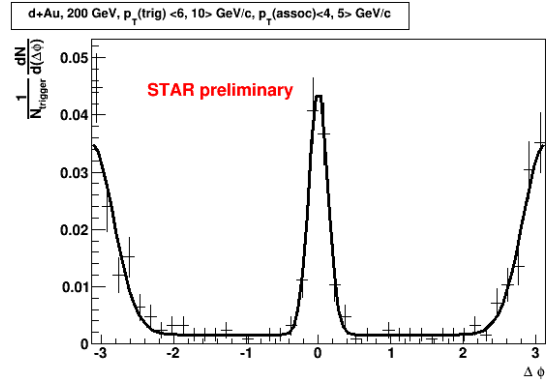


Figure 25: Azimuthal correlation with  $p_T(\text{trig}) <6,10>$  GeV,  $p_T(\text{assoc}) <4,5>$  GeV.

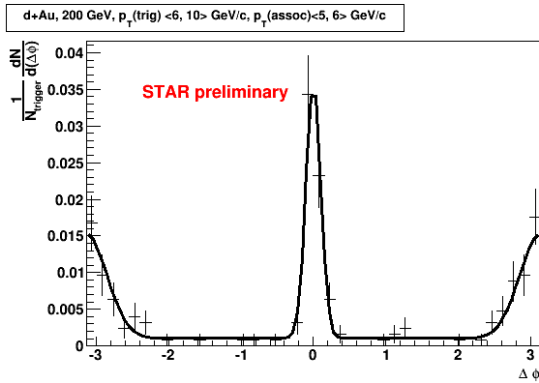


Figure 26: Azimuthal correlation with  $p_T(\text{trig}) <6,10>$  GeV,  $p_T(\text{assoc}) <5,6>$  GeV.

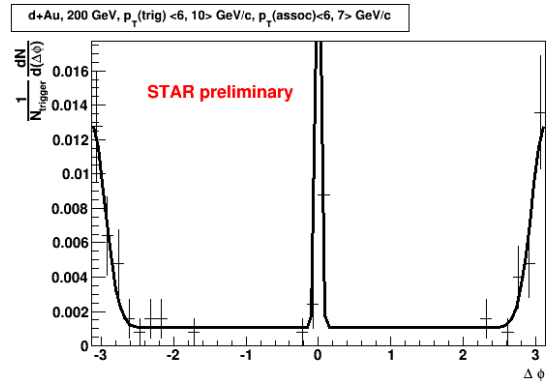


Figure 27: Azimuthal correlation with  $p_T(\text{trig}) <6,10>$  GeV,  $p_T(\text{assoc}) <6,7>$  GeV.

In previous figures we can see that both peaks, from the near-side jet and from the away-side jet, have almost the same height. Small differences are due to the fact that in the near-side peak contains the trigger particle (particle with the highest  $p_T$ ). Differences between peaks seen in Figure 16, 19, 20, 21, 26, are caused by growing values of  $p_T^{trig}$ . The shape of the away-side peak in  $p + p$  and  $d + Au$  collisions is almost identical (correlations have the same characteristics). In all figures 14-27 the away-side peaks are wider when compared to the near-side peaks. This is due to the  $k_T$  effect which will we study in diploma thesis.

### The near- and away-side yields

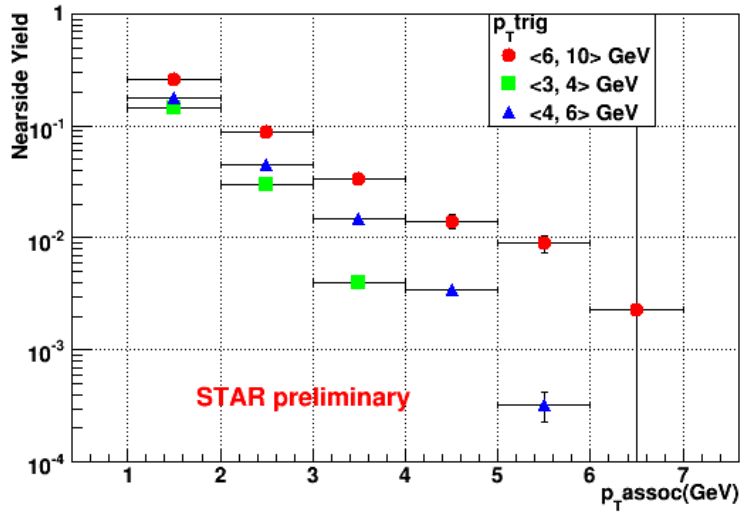


Figure 28: Dependence of near-side yield on  $p_T^{assoc}$  for various  $p_T^{trig}$  ranges.

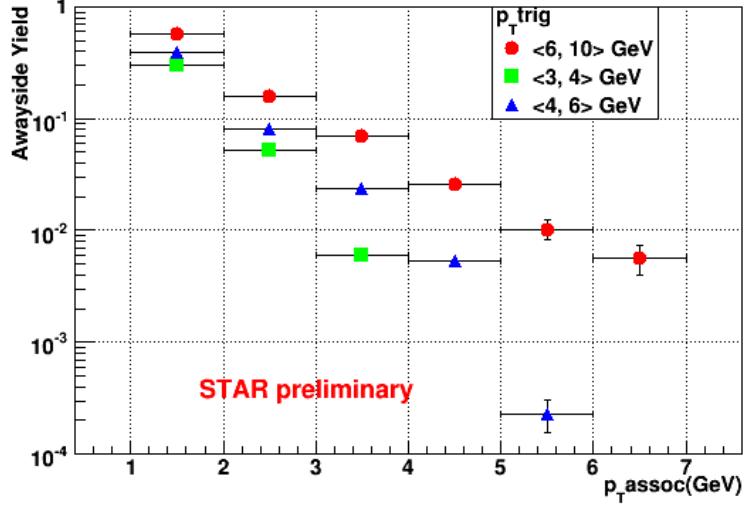


Figure 29: Dependence of away-side yield on  $p_T^{assoc}$  for various  $p_T^{trig}$  ranges.

Figure 28, 29 show the dependence of near- and away-side yield on  $p_T^{assoc}$  for the  $p_T^{trig}$  ranges of figures 14-27. Single value of yields are calculated from figures 14-27 like a result of amplitude and width of corresponding peaks: away-side yield =  $p_0|p_1|\sqrt{2\pi}$ , near-side yield =  $p_2|p_3|\sqrt{2\pi}$ .

It is known now that the near- and away-side yields decrease with increasing values of  $p_T^{assoc}$ . Away-side peak strongly depends on system size and on collision centrality[16].

## 5 Summary and Conclusion

The main goal of the research project was a study of azimuthal correlations of hadrons with high transverse momentum in nucleus-nucleus collisions, and their practical application on data from d+Au collisions at  $\sqrt{s_{NN}} = 200$  GeV measured by the STAR collaboration at RHIC in 2008.

The results of the analysis show that the correlations have the same characteristics in d+Au collisions and in p+p collisions. In order to study the phenomena in the medium (produced during collision), we need to measure them in a reference system. The natural choice would be p+p or more suitable d+Au collisions (larger statistics). In d+Au collisions significant suppression of high  $p_T$  particles is not observed in comparison with Au+Au collisions caused i.a. by energy loss of light partons in dense nuclear matter. This suppression is not caused by nuclear effects in the initial state, but in the final state by interaction of hard scattered parton or fragmentation products with dense matter formed in the collision. This fact points to a jet energy loss in nuclear matter produced in Au+Au collisions.

## References

- [1] <http://www.bnl.gov/rhic>.
- [2] K.Yagi et al., Quark-Gluon Plasma, Cambridge University Press (2005).
- [3] <http://www4.rcf.bnl.gov/brahms/WWW/overview.html>.
- [4] <http://drupal.star.bnl.gov/STAR/public/img>.
- [5] K.H. Ackermann et al., Nuclear Instruments and Methods in Physics Research A 499 (2003) 624–632.
- [6] M. Sloboda, Bachelor’s Thesis, Czech Technical University in Prague, (2008).
- [7] M. Anderson et al., Nuclear Instruments and Methods in Physics Research A 499 (2003) 659–678.
- [8] M. Beddo et al., Nucl. Instrum. Meth. A 499, 725 (2003).
- [9] W. J. Llope et al., arXiv:nucl-ex/0308022v1.
- [10] C. Chasman, D. Beavis et al., STAR Collaboration. A Heavy Flavor Tracker for STAR (2009).
- [11] <http://press.web.cern.ch/press/PressReleases/Releases2000/PR01.00EQuarkGluonMatter.html>.
- [12] STAR Collaboration, Evidence from d+Au measurements for final-state suppression of high  $p_T$  hadrons in Au+Au collisions at RHIC, Phys.Rev.Lett.91:072304, (2003), arXiv:nucl-ex/0306024v3.
- [13] C. Adler et al., Phys. Rev. Lett., arXiv:nucl-ex/0210033v1.
- [14] Run 2008 info, <http://www.star.bnl.gov/protected/common/common2008/trigger2008/triggers2008.html>.
- [15] C. Adler et al., The RHIC Zero Degree Calorimeters, arXiv:nucl-ex/0008005v1.
- [16] STAR Collaboration, System size dependence of associated yields in hadron-triggered jets, Phys.Lett.B683:123-128, (2010), arXiv:0904.1722.